AJR FOCUS ON:

An Approach to the Evaluation of Incidentally Identified Bone Lesions Encountered on Imaging Studies

Stephanie Bernard[1]
Eric Walker[1]
Meera Raghavan[2,3]

OBJECTIVE. This article discusses the strengths and weaknesses of the various anatomic and molecular imaging techniques in the evaluation of unexpected bone lesions.

CONCLUSION. An approach to the imaging evaluation of chondroid, osteoblastic, and osteolytic lesions as well as focal marrow abnormalities is reviewed.

Keywords: bone lesion, incidental finding, osteoblastic, osteolytic, unexpected

DOI:10.2214/AJR.16.17434

Received September 26, 2016; accepted without revision October 7, 2016.

Based on presentations at the ARRS 2014 Annual Meeting (San Diego, CA) and the ARRS 2015 Annual Meeting (Toronto, ON, Canada).

[1]Department of Radiology, Penn State Hershey Medical Center, 500 University Dr, Hershey, PA 17033. Address correspondence to S. Bernard (sbernard@hmc.psu.edu).

[2]Department of Radiology, Moffitt Cancer Center, Tampa, FL.

[3]Present address: Department of Radiology, Division of Nuclear Medicine and Molecular Imaging, Northwell Health, New Hyde Park, NY.

This article is available for credit.

AJR 2017; 208:960–970

0361–803X/17/2085–960

Unexpected bone lesions present a common diagnostic dilemma. The overall frequency of unexpected musculoskeletal findings in retrospective reviews is 2–10% [1–4]. When faced with unexpected findings, the goal is to accurately distinguish which lesions can be safely ignored from those requiring additional workup or biopsy. As part of this process, understanding the strengths and limitations of the various imaging tests when applied to commonly encountered scenarios is essential for selecting the most cost-effective and expeditious workup. For the unexpected bone lesions, the distinguishing anatomic features and a generalized imaging approach will be reviewed for four frequently encountered scenarios: chondroid lesions, sclerotic bone lesions, osteolytic lesions, and areas of focal marrow abnormality.

General Considerations

If a bone lesion is being first encountered at MRI, conventional radiographs should be obtained for comparison. The radiographs will allow evaluation of the key features of the bone lesion, including its margin, periosteal reaction, and matrix. A full discussion of the systematic radiographic assessment of bone lesions has been well covered in prior publications [5–8]. A key concept is that the radiographic appearance of a bone lesion's margin is a direct reflection of the lesion's biologic aggressiveness, with a sclerotic margin radiographically reflecting indolent growth that has allowed adjacent bone repair. As such, a well-defined sclerotically marginated lesion radiographically has a less than 6% chance of malignancy, whereas a geographic osteolytic lesion with a partially ill-defined margin has a likelihood of malignancy that approaches 50%, and a permeative lesion has a greater than 80% likelihood of malignancy [9].

Lesion matrix can help recognize primary cartilaginous, osseous, or fibrous bone tumors [8]. This mineralized matrix may be quite difficult to recognize at MRI. The differential considerations for a bone lesion will be based on the aggressiveness of the lesion and the presence or absence of a specific matrix, coupled with the patient's age and the location of the lesion in bone both longitudinally and axially [8, 10]. It should be remembered that primary bone sarcomas are relatively rare, representing less than 0.2% of bone malignancies [11]. Metastatic disease, multiple myeloma, lymphoma, and leukemia account for more than 99% of malignant bone lesions. Of the metastatic lesions, 85% originate from five primary sites: breast, lung, prostate, kidney, and thyroid [12]. It is important when faced with a localized bone lesion to form the initial differential diagnosis considering all categories of disease (neoplasm, infectious, inflammatory, trauma, congenital or developmental, endocrine or metabolic, vascular, drug effect, and autoimmune or collagen vascular) to prevent overlooking the sometimes unusual but correct diagnosis.

Scenario 1: Chondroid Lesions

Osteochondroma Versus Exostotic Chondrosarcoma

Osteochondromas are the most common benign neoplasms of bone, representing 10–

15% of all primary bone tumors and up to 50% of benign bone lesions [13]. The osteochondroma is an exophytic growth from the bone that shows the diagnostic imaging features of cortical and medullary continuity with the underlying bone [13]. Osteochondromas may present as a mass or because of secondary complications, such as adventitial bursal formation, compression of adjacent structures, or fracture [13, 14]. Malignant transformation of the cartilage cap into a secondary chondrosarcoma varies from less than 1% for solitary osteochondromas to 2–5% in cases of hereditary multiple exostosis [13]. Even in patients with hereditary multiple exostosis, malignant transformation is rare before age 20 years [13, 15, 16]. Several authors have noted an increased rate of malignant transformation of osteochondromas arising from the axial skeleton [14, 17–19]. When a secondary chondrosarcoma develops from an osteochondroma, 85% or more will be grade 1 tumors with a very low metastatic potential [20–22].

Cartilage has a high fluid content. The cartilage cap shows low echogenicity on ultrasound, an attenuation slightly above that of water on CT, and an MRI appearance of intermediate-to-low signal on T1-weighted images and intermediate-to-high signal on T2-weighted images, all reflecting the fluid content [13]. IV contrast-enhanced imaging will show a peripheral and septal enhancement pattern of the cartilage surface [13]. Chondrosarcomatous transformation is best identified through measurement of a cartilage cap thickness of 2 cm or greater [20] (Fig. 1). Pain and a rapid increase in lesion size after adolescence suggest a malignant transformation in a patient with a previously asymptomatic osteochondroma [13]. An artifactually thickened appearance can be created by a fluid-filled adventitial bursa at sites of osteochondroma friction with adjacent structures, most commonly encountered with ventral scapular or hip osteochondromas [23]. Because the bursa will also show fluid signal with peripheral enhancement on contrast-enhanced imaging, MRI sequences that provide contrast distinction between the cartilage cap and free fluid in the bursa, such as a cartilage-sensitive fat-suppressed spoiled gradient-echo sequence, can be helpful in making the distinction [13, 20].

FDG PET/CT has been found to reveal increased glucose metabolism in lesions with grade 2 (standardized uptake value [SUV], 2.4–4.6) or grade 3 chondrosarcoma (SUV, 6–20) or foci of dedifferentiation (SUV, 11.4) [16]. However, PET shows similar SUVs for benign osteochondromas (SUV, 0.9–1.3) and grade 1 chondrosarcomas (SUV, 1.4–3.4). Because grade 1 tumors comprise the bulk of the chondrosarcomas arising from osteochondromas, FDG PET does not provide useful differentiation in most cases.

Enchondromas Versus Conventional Chondrosarcoma

Enchondromas are quite common, representing 10–25% of all benign bone tumors [24]. Enchondromas are thought to be the result of the continued growth of residual benign cartilaginous rests that are displaced from the growth plate [10, 25]. Lesions smaller than 1 cm are referred to as "cartilage rests."

Enchondromas are uncommon in the spine and pelvis and deserve additional scrutiny as potential chondrosarcomas [25]. Proximal to the hands and feet, many enchondromas will show arc-and-ring or stippled chondroid matrix radiographically or at CT. Enchondromas often show a characteristic lobular growth pattern and, because of the high fluid content of cartilage, are intermediate-to-low signal on T1-weighted images and intermediate-to-high signal on T2-weighted images in the regions not calcified [23]. When faced with an indeterminate marrow-replacing lesion approaching fluid signal on T1- and T2-weighted images, T1-weighted fat-suppressed imaging after IV gadolinium contrast administration can be helpful in recognizing the characteristic lobular, peripheral, and septal enhancement pattern of a chondroid lesion [10, 25].

Imaging features that are useful in distinguishing intramedullary chondrosarcoma from enchondroma include endosteal scalloping of greater than two-thirds cortical depth, cortical remodeling, cortical destruction, periosteal reaction, size larger than 5 cm, and soft-tissue mass [25–27] (Figs. 2 and 3). With the caveat that cortical remodeling and bone expansion is not a reliable discriminator in narrow tubular bones such as the fibula or bones of the hands and feet, all of these features otherwise strongly suggest the diagnosis of chondrosarcoma [25, 28].

Pain is the most common presenting symptom of chondrosarcoma, observed in 95% of patients, and may be the only distinguishing feature in low-grade chondrosarcomas [25, 26, 29]. For lesions lacking the more-aggressive radiographic features discussed already, distinction of the pain from an adjacent joint pathologic abnormality may be accomplished with intraarticular lidocaine injection [25, 28]. For those without relief of pain, where the clinical concern remains a potential low-grade chondrosarcoma, the lesion can be safely followed for stability, because low-grade chondrosarcomas are slow growing and have a very low metastatic potential [30]. If biopsy is going to be performed, it should be done surgically as an excisional biopsy, because a percutaneous biopsy specimen will be insufficient for excluding a low-grade chondrosarcoma [29]. Percutaneous biopsy should be conserved for more-aggressive higher-grade lesions to establish a diagnosis and allow definitive surgical treatment [25].

Uptake of radionuclide greater than that of the anterior iliac crest at bone scintigraphy is seen in 82% of chondrosarcomas [25]. Most enchondromas show uptake less than or equal to that of the anterior iliac crest but there is overlap [31]. FDG PET/CT may be helpful in distinguishing low-grade chondrosarcoma from enchondroma using a recommended pretherapeutic SUV greater than 2.0 as being suspicious for malignancy and an SUV greater than 2.2 to improve specificity [32, 33]. The appearance anatomically, however, remains the primary means of differentiation of enchondroma and chondrosarcoma.

Scenario 2: Sclerotic Lesion

Enostosis Versus Sclerotic Metastasis

When faced with any isolated sclerotic focus in bone, one of the first considerations is whether the lesion could represent an enostosis or bone island. The enostosis represents a benign hamartoma of cortical bone most frequently seen in the spine, pelvis, and epiphyses or metaphyses of the long bones. Enostoses are common, present in up to 14% of patients on autopsy series [34]. There are certain features by cross-sectional imaging characteristic of enostoses. Because they are composed of compact bone, enostoses are expected to be homogeneously as dense as cortical bone radiographically and at CT. The enostosis will often show a spiculated or thorny margin that blends with the adjacent trabecula or cortex [35, 36]. When reexamined on serial imaging, as many as 31% of enostoses will change in size [37]. The diameter of their growth, however, is expected to show a less than 25% increase in size over 6 months or 50% in 1 year. Biopsy should be considered for any lesion exceeding this growth rate [36].

TABLE 1: Common Radiographic Appearance of Adult Metastatic Bone Lesions by Source

Osteoblastic	Mixed Lytic and Blastic	Osteolytic
Prostate	Lung	Lung
Breast	Breast	Renal
Carcinoid	Cervical	Thyroid
	Bladder	Most squamous cell cancers
	Testicular	Melanoma
	Gastrointestinal	Hepatocellular
		Colon
		Bladder

The enostosis should be homogeneously low signal on all MRI pulse sequences, similar to cortical bone, with the marrow contacting the margin of an enostosis normal in signal on all pulse sequences [35, 36, 38]. On ^{99m}Tc–methylene diphosphonate bone scans, most enostoses will show radiotracer accumulation similar to that of background bone [35, 36]. However, enostoses may be warm or even hot on bone scans [36, 39–41].

There are a few primary carcinomas that produce purely sclerotic bone metastases that may mimic an enostosis (Table 1). The most common sources of sclerotic metastases are breast and prostate carcinomas. At CT, the differentiation of a sclerotic metastasis from an enostosis when small may be quite difficult without multifocal identifiable disease (Fig. 4). As the lesions enlarge, metastases may show less-homogeneous internal attenuation than cortical bone. An MRI finding that should raise concern for a sclerotic bone metastasis is a rim of abnormal increased T2 signal in the surrounding marrow, a finding termed a "halo sign" (Fig. 5). Although it is not present in all sclerotic metastases, when encountered, the halo sign should prompt biopsy because there is a reported 99% specificity of this finding for metastasis [42].

The past recommendation for evaluation of a sclerotic bone lesion thought to potentially represent an enostosis was to perform bone scintigraphy [43]. Those lesions with an appropriate radiographic or cross-sectional appearance and with tracer accumulation similar to that of background bone were accepted as being consistent with enostosis. On the basis of a meta-analysis, planar bone scintigraphy has a sensitivity for an individual sclerotic metastasis of approximately 59%, which can be improved to 90% with SPECT imaging [44] (Table 2). With the overlap of potential warm or hot enostoses and a false-negative rate for axial sclerotic bone metastases on planar bone scintigraphy of up to 40%, planar bone scintigraphy should not be used to either exclude or mandate a need for biopsy of any individual sclerotic lesion. The strength of bone scintigraphy is the relatively inexpensive widely accessible whole-skeleton screening it provides. This screening can show the presence and distribution of additional lesions that can be helpful in recognize the pathologic abnormality as metastatic (Fig. 4C). Although it is not widely available currently, ^{18}F-NaF-PET/CT shows an improved ability to detect sclerotic bone metastases when compared with bone scintigraphy, with sensitivities above 90% [45]. For bone scintigraphy not performed as SPECT/CT, lesions will require radiographic correlation at sites of tracer accumulation to separate traumatic, arthropathy-related, or other benign bone lesion causes.

Prostate Cancer

Prostate cancer is the second most common malignancy in men [12]. At diagnosis, the differentiation of localized from metastatic prostate cancer is critical for determining those patients eligible for localized treatment versus those needing systemic therapy. The urologic literature is currently debating the most appropriate bone imaging study for prostate cancer staging on the basis of the improved accuracy of ^{18}F-NaF-PET/CT and whole-body MRI in comparison with bone scintigraphy in early identification of bone metastases [46–49] (Fig. 6).

The likelihood of bone metastasis can be predicted on the basis of the prostate-specific antigen (PSA) level, Gleason score, and clinical stage [50]. Poorly differentiated tumors may not produce PSA and, therefore, all require bone scintigraphy or ^{18}F-NaF-PET/CT. For the remainder of moderately to well-differentiated tumors, there are published odds ratios available for the risk of bone metastases based on this algorithm [51]. A PSA level of less than 10 ng/mL in a patient with well or moderately differentiated tumor, in the absence of specific bone symptoms, has a 99% negative predictive value for bone metastasis, whereas a PSA level greater than 100 ng/mL has a nearly 100% positive predictive value. Current recommendations are for initial screening with bone scintigraphy in patients with PSA levels over 20 ng/mL [52].

Breast Cancer

Breast cancer represents the most common malignancy in women [12]. Although most identified bone lesions will follow the approach to evaluation already discussed in this review, a special caveat deserves mention—the isolated sternal lesion. Skeletal metastatic disease from all causes is multifocal in 90% of patients, with up to 21% of breast cancers presenting with a solitary bone metastasis. Solitary rib lesions in all patients with an established malignancy of any cause carries a risk of representing metastatic disease of approximately 10% [53]. Although isolated sternal metastases are uncommon in most malignancies, in a patient with an established diagnosis of breast cancer, an isolated sternal lesion has a 76% likelihood of

TABLE 2: Nuclear Medicine Imaging Sensitivity in Detection of Bone Metastatic Disease

	Bone Scintigraphy (SPECT)		FDG PET/CT		^{18}F-NaF-PET/CT	
Type of Imaging	Lytic	Blastic	Lytic	Blastic	Lytic	Blastic
Sensitivity (%)	50–80[a]	85–95	95–100[b]	56–85[c]	89–95	95–100

[a]Sensitivity can be as low as 10% for renal cell metastases but improves with hybrid SPECT/CT.
[b]Sensitivity is less than 85% in low metabolic tumors including multiple myeloma and differentiated thyroid carcinoma.
[c]Performs worse in purely osteoblastic lesions.

representing a metastasis and warrants biopsy [54]. Because the isolated sternal metastasis may be surgically treated, if no other lesions are identified on bone scintigraphy, ^{18}F-NaF-PET/CT should be considered for improved detection of additional metastases that would alter treatment planning [55].

Scenario 3: Focal Osteolytic Lesion—Benign Versus Malignant

In addition to multiple myeloma and lymphoma, the metastases that most commonly present as osteolytic lesions in adults include lung, renal, and thyroid carcinomas (Table 1), but there are a variety of nonmalignant bone lesions, including enchondromas, that may present as focal nonsclerotically marginated or indeterminant osteolytic lesions.

When faced with an osteolytic lesion, radiographs will be helpful in determining the initial aggressiveness of the lesion and the need for additional workup. An asymptomatic lesion with a nonaggressive sclerotic margin in the absence of a history of treated malignancy requires no additional imaging. For indeterminant lesions, MRI is the most helpful next step in local characterization. An MRI feature that can be helpful in excluding malignancy in a bone lesion is the identification of macroscopic fat, a finding that carries with it a 99.5% likelihood of the lesion being benign [42].

For those lesions lacking identifiable benign MRI features, FDG PET/CT can be helpful in stratifying lesions that warrant biopsy from those that can be followed. FDG PET/CT has a sensitivity for metastatic bone lesions and lymphoma of approximately 95% [56–59]. The sensitivity is lower for multiple myeloma, reported in the literature as ranging from 59% to 85% [60, 61]. Similarly, differentiated thyroid cancer can have a low metabolic rate and a similarly lower overall detection rate on FDG PET of approximately 85%, stressing the importance of concomitant anatomic imaging evaluation [62].

Follow-up instead of biopsy is reasonable in lesions lacking metabolic activity on FDG PET/CT, in conjunction with negative serum electrophoresis for a gammaglobulinopathy (Fig. 7). When metabolic activity with SUV greater than 2 is present, the differential diagnosis continues to include benign tumors, trauma, and infectious or inflammatory diseases that may present as false-positives for malignancy [63]. The combined CT examination improves the specificity, allowing anatomic recognition of benign causes of activity while also allowing evaluation for extraskeletal soft-tissue lesions and sources of primary malignancy.

Bone scintigraphy is less sensitive for osteolytic lesions, with reported sensitivities as low as 50% because of a lack of activation of osteoblastic activity by some tumors [64]. Fluorine-18-NaF-PET/CT also localizes to bone repair with improved pharmacokinetics and imaging system resolution in comparison with bone scintigraphy, resulting in twice as many osteolytic lesions being detected, but it still is significantly less sensitive than FDG PET/CT in multiple myeloma [65, 66].

Scenario 4: Focal Marrow Abnormality on MRI—Red Marrow Versus Malignancy

There is a normal predictable pattern of conversion from red (hematopoietic) marrow to yellow (fatty) marrow from infancy to adult life. The epiphyses and epiphyseal equivalents develop yellow marrow with ossification in the first year of life [67, 68]. The long bones then undergo a conversion from red to yellow marrow beginning in the diaphyses and extending toward the metaphyses, with clearance of red marrow occurring quicker distally than proximally. By approximately age 25 years, an adult pattern of red marrow that is primarily confined to the axial skeleton and in islands in the metaphyses of the proximal long bones is seen [67–70]. When faced with increased demands for production, red marrow reconversion occurs in the opposite sequence, first in the proximal followed by the distal metaphyses, with later progression into the diaphysis [71]. The epiphyses and epiphyseal equivalents are the last to undergo reconversion. Marrow is best assessed in patients older than 1 year on T1-weighted MR images with STIR images for support. Because of the intermixed microscopic marrow fat contained within hematopoietic marrow, normal marrow will be higher in signal than muscle on T1-weighted images or, when evaluating the spine, higher in signal than disk on T1-weighted images [68, 72].

Focal marrow abnormalities encountered incidentally at MRI may present a conundrum. As with radiographic osteolytic lesions, a search for the presence of macroscopic fat within the lesion should be performed because lesions containing macroscopic fat are invariably benign [42]. Focal red marrow can occasionally appear masslike and may not have macroscopically visible fat. When faced with a focal area that is approaching intermediate signal (equivalent to skeletal muscle) at MRI, in-phase and out-of-phase T1-weighted gradient images may be helpful in differentiating islands of red marrow from myeloma or metastases [73]. Just as these sequences are used for recognition of microscopic fat in an adrenal adenoma, the microscopic fat admixed within red marrow will result in a decrease in signal on the out-of-phase images when compared with the signal change in skeletal muscle (Fig. 8). Tumor cells, in contrast, multiply and displace the normal marrow fat. These metastases will show India ink artifact on out-of-phase imaging along their interface with marrow but will lack the central lesional signal decrease.

If the focal marrow abnormality cannot be shown to contain macroscopic or microscopic fat, approximately 6% will eventually be diagnosed as malignancy [2, 74]. It is prudent to start with a search of the patient's medical record for history, physical examination and laboratory findings, and imaging for screening already performed for the malignancies most likely to cause focal marrow lesions, which are breast cancer, lung cancer, lymphoma, and multiple myeloma [74]. If not already performed, laboratory tests and a screening chest radiograph or mammogram would be a reasonable first step. The study often most helpful is an FDG PET/CT. Not only does it provide whole-body screening both anatomically and metabolically, it has an approximately 95% sensitivity for identifying metastatic lesions and lymphoma, as described elsewhere [56–59]. As such, it is helpful in stratifying lesions into a need for biopsy versus those that can be followed. Occasionally, the focal marrow abnormality is first encountered on FDG PET/CT. Focal FDG metabolic activity in the absence of an anatomic lesion on CT carries a 61% chance of metastatic disease as the underlying cause and warrants further clinical screening and potentially biopsy [75].

Risk of Pathologic Fracture

A common clinical concern when a bone lesion is identified is the risk for pathologic fracture. The most widely applied criteria for the prediction of pathologic fracture risk are the Mirels classification [76, 77]. There are four criteria considered predictive, with 1–3 points assigned to each (Fig. 9). These criteria include, first, whether the lesion is osteoblastic, mixed osteolytic and osteoblastic, or osteolytic; second, whether the location of the lesion is in the upper extremity, lower extremity, or peritrochanteric region; third, whether the cortical involvement is less than one-third

of the diameter, up to two-thirds of the diameter, or greater than two-thirds of the diameter; and fourth, whether the associated pain is mild, moderate, or functional. Fracture risk increases exponential with scores over 7, with scores of 9 points or more generally considered an indication for prophylactic fixation.

Bone Biopsies

If, after workup, biopsy is required, it is crucial that any isolated bone lesion be approached as a primary sarcoma until proven otherwise, to avoid contamination of tissue planes that would preclude the surgeon from being able to offer the patient limb-sparing surgery. There are published general principles and biopsy approaches that will prevent inappropriate access through muscles and neurovascular planes that must be avoided. These have been well illustrated in a prior article that should be reviewed before undertaking bone biopsies [78]. Foremost, however, biopsy planning must involve direct consultation with the surgeon who will be removing the tumor because, occasionally, the reconstruction plan will involve a rotational muscle flap that would be violated by the typically described biopsy tracks, thus requiring a deviation from the expected biopsy approach.

References

1. Grainger R, Stuckey S, O'Sullivan R, Davis SR, Ebeling PR, Wluka AE. What is the clinical and ethical importance of incidental abnormalities found by knee MRI? *Arthritis Res Ther* 2008; 10:R18
2. Hegenscheid K, Seipel R, Schmidt CO, et al. Potentially relevant incidental findings on research whole-body MRI in the general adult population: frequencies and management. *Eur Radiol* 2013; 23:816–826
3. Morin SH, Cobbold JF, Lim AK, et al. Incidental findings in healthy control research subjects using whole-body MRI. *Eur J Radiol* 2009; 72:529–533
4. Park HJ, Jeon YH, Rho MH, et al. Incidental findings of the lumbar spine at MRI during herniated intervertebral disk disease evaluation. *AJR* 2011; 196:1151–1155
5. Sweet DE, Madewell JE, Ragsdale BD. Radiologic and pathologic analysis of solitary bone lesions. Part III. Matrix patterns. *Radiol Clin North Am* 1981; 19:785–814
6. Ragsdale BD, Madewell JE, Sweet DE. Radiologic and pathologic analysis of solitary bone lesions. Part II. Periosteal reactions. *Radiol Clin North Am* 1981; 19:749–783
7. Madewell JE, Ragsdale BD, Sweet DE. Radiologic and pathologic analysis of solitary bone lesions. Part I. Internal margins. *Radiol Clin North Am* 1981; 19:715–748
8. Miller TT. Bone tumors and tumorlike conditions: analysis with conventional radiography. *Radiology* 2008; 246:662–674
9. Caracciolo JT, Temple HT, Letson GD, Kransdorf MJ. A modified Lodwick-Madewell grading system for the evaluation of lytic bone lesions. *AJR* 2016; 207:150–156
10. Johnson LC. A general theory of bone tumors. *Bull N Y Acad Med* 1953; 29:164–171
11. Howlader NNA, Krapcho M, Miller D, et al. SEER cancer statistics review (CSR) 1975–2013. National Cancer Institute website. seer.cancer.gov/csr/1975_2013/. Published April 2016. Updated September 12, 2016. Accessed December 21, 2016
12. American Cancer Society. *Cancer facts and figures 2016*. Atlanta, GA: American Cancer Society, 2016
13. Murphey MD, Choi JJ, Kransdorf MJ, Flemming DJ, Gannon FH. Imaging of osteochondroma: variants and complications with radiologic-pathologic correlation. *RadioGraphics* 2000; 20:1407–1434
14. Lee KC, Davies AM, Cassar-Pullicino VN. Imaging the complications of osteochondromas. *Clin Radiol* 2002; 57:18–28
15. Ozaki T, Hillmann A, Blasius S, Link T, Winkelmann W. Multicentric malignant transformation of multiple exostoses. *Skeletal Radiol* 1998; 27:233–236
16. Purandare NC, Rangarajan V, Agarwal M, et al. Integrated PET/CT in evaluating sarcomatous transformation in osteochondromas. *Clin Nucl Med* 2009; 34:350–354
17. Ahmed AR, Tan TS, Unni KK, Collins MS, Wenger DE, Sim FH. Secondary chondrosarcoma in osteochondroma: report of 107 patients. *Clin Orthop Relat Res* 2003; 193–206
18. Solomon L. Chondrosarcoma in hereditary multiple exostosis. *S Afr Med J* 1974; 48:671–676
19. Wuisman PI, Jutte PC, Ozaki T. Secondary chondrosarcoma in osteochondromas: medullary extension in 15 of 45 cases. *Acta Orthop Scand* 1997; 68:396–400
20. Bernard SA, Murphey MD, Flemming DJ, Kransdorf MJ. Improved differentiation of benign osteochondromas from secondary chondrosarcomas with standardized measurement of cartilage cap at CT and MR imaging. *Radiology* 2010; 255:857–865
21. Evans HL, Ayala AG, Romsdahl MM. Prognostic factors in chondrosarcoma of bone: a clinicopathologic analysis with emphasis on histologic grading. *Cancer* 1977; 40:818–831
22. Garrison RC, Unni KK, McLeod RA, Pritchard DJ, Dahlin DC. Chondrosarcoma arising in osteochondroma. *Cancer* 1982; 49:1890–1897
23. Douis H, Saifuddin A. The imaging of cartilaginous bone tumours. Part I. Benign lesions. *Skeletal Radiol* 2012; 41:1195–1212
24. Logie CI, Walker EA, Forsberg JA, Potter BK, Murphey MD. Chondrosarcoma: a diagnostic imager's guide to decision making and patient management. *Semin Musculoskelet Radiol* 2013; 17:101–115
25. Murphey MD, Flemming DJ, Boyea SR, Bojescul JA, Sweet DE, Temple HT. Enchondroma versus chondrosarcoma in the appendicular skeleton: differentiating features. *RadioGraphics* 1998; 18:1213–1237; quiz, 1244–1215
26. Ferrer-Santacreu EM, Ortiz-Cruz EJ, Gonzalez-Lopez JM, Perez Fernandez E. Enchondroma versus low-grade chondrosarcoma in appendicular skeleton: clinical and radiological criteria. *J Oncol* 2012; 2012:437958
27. Geirnaerdt MJ, Hermans J, Bloem JL, et al. Usefulness of radiography in differentiating enchondroma from central grade 1 chondrosarcoma. *AJR* 1997; 169:1097–1104
28. Kendell SD, Collins MS, Adkins MC, Sundaram M, Unni KK. Radiographic differentiation of enchondroma from low-grade chondrosarcoma in the fibula. *Skeletal Radiol* 2004; 33:458–466
29. Wang XL, De Beuckeleer LH, De Schepper AM, Van Marck E. Low-grade chondrosarcoma vs enchondroma: challenges in diagnosis and management. *Eur Radiol* 2001; 11:1054–1057
30. Crim J, Schmidt R, Layfield L, Hanrahan C, Manaster BJ. Can imaging criteria distinguish enchondroma from grade 1 chondrosarcoma? *Eur J Radiol* 2015; 84:2222–2230
31. Flemming DJ, Murphey MD. Enchondroma and chondrosarcoma. *Semin Musculoskelet Radiol* 2000; 4:59–71
32. Feldman F, Van Heertum R, Saxena C, Parisien M. ^{18}FDG-PET applications for cartilage neoplasms. *Skeletal Radiol* 2005; 34:367–374
33. Jesus-Garcia R, Osawa A, Filippi RZ, et al. Is PET-CT an accurate method for the differential diagnosis between chondroma and chondrosarcoma? *Springerplus* 2016; 5:236
34. Resnick D, Nemcek AA Jr, Haghighi P. Spinal enostoses (bone islands). *Radiology* 1983; 147:373–376
35. Greenspan A. Bone island (enostosis): current concept—a review. *Skeletal Radiol* 1995; 24:111–115
36. Greenspan A, Steiner G, Knutzon R. Bone island (enostosis): clinical significance and radiologic and pathologic correlations. *Skeletal Radiol* 1991; 20:85–90
37. Onitsuka H. Roentgenologic aspects of bone islands. *Radiology* 1977; 123:607–612
38. Murphey MD, Andrews CL, Flemming DJ, Temple HT, Smith WS, Smirniotopoulos JG. From the archives of the AFIP: primary tumors of the spine—radiologic pathologic correlation. *RadioGraphics* 1996; 16:1131–1158
39. Go RT, El-Khoury GY, Wehbe MA. Radionuclide bone image in growing and stable bone island.

Skeletal Radiol 1980; 5:15–18

40. Gold RH, Mirra JM, Remotti F, Pignatti G. Case report 527: giant bone island of tibia. *Skeletal Radiol* 1989; 18:129–132
41. Hall FM, Goldberg RP, Davies JA, Fainsinger MH. Scintigraphic assessment of bone islands. *Radiology* 1980; 135:737–742
42. Schweitzer ME, Levine C, Mitchell DG, Gannon FH, Gomella LG. Bull's-eyes and halos: useful MR discriminators of osseous metastases. *Radiology* 1993; 188:249–252
43. Greenspan A, Stadalnik RC. Bone island: scintigraphic findings and their clinical application. *Can Assoc Radiol J* 1995; 46:368–379
44. Shen G, Deng H, Hu S, Jia Z. Comparison of choline-PET/CT, MRI, SPECT, and bone scintigraphy in the diagnosis of bone metastases in patients with prostate cancer: a meta-analysis. *Skeletal Radiol* 2014; 43:1503–1513
45. Bastawrous S, Bhargava P, Behnia F, Djang DS, Haseley DR. Newer PET application with an old tracer: role of ^{18}F-NaF skeletal PET/CT in oncologic practice. *RadioGraphics* 2014; 34:1295–1316
46. Kjölhede H, Ahlgren G, Almquist H, et al. Combined ^{18}F-fluorocholine and ^{18}F-fluoride positron emission tomography/computed tomography imaging for staging of high-risk prostate cancer. *BJU Int* 2012; 110:1501–1506
47. Beheshti M, Vali R, Waldenberger P, et al. Detection of bone metastases in patients with prostate cancer by ^{18}F fluorocholine and ^{18}F fluoride PET-CT: a comparative study. *Eur J Nucl Med Mol Imaging* 2008; 35:1766–1774
48. Brogsitter C, Zophel K, Kotzerke J. ^{18}F-Choline, ^{11}C-choline and ^{11}C-acetate PET/CT: comparative analysis for imaging prostate cancer patients. *Eur J Nucl Med Mol Imaging* 2013; 40(suppl 1):S18–S27
49. Langsteger W, Balogova S, Huchet V, et al. Fluorocholine (18F) and sodium fluoride (18F) PET/CT in the detection of prostate cancer: prospective comparison of diagnostic performance determined by masked reading. *Q J Nucl Med Mol Imaging* 2011; 55:448–457
50. Briganti A, Passoni N, Ferrari M, et al. When to perform bone scan in patients with newly diagnosed prostate cancer: external validation of the currently available guidelines and proposal of a novel risk stratification tool. *Eur Urol* 2010; 57:551–558
51. McArthur C, McLaughlin G, Meddings RN. Changing the referral criteria for bone scan in newly diagnosed prostate cancer patients. *Br J Radiol* 2012; 85:390–394
52. Roberts CC, Daffner RH, Weissman BN, et al. ACR appropriateness criteria on metastatic bone disease. *J Am Coll Radiol* 2010; 7:400–409
53. Tumeh SS, Beadle G, Kaplan WD. Clinical significance of solitary rib lesions in patients with extraskeletal malignancy. *J Nucl Med* 1985; 26:1140–1143
54. Kwai AH, Stomper PC, Kaplan WD. Clinical significance of isolated scintigraphic sternal lesions in patients with breast cancer. *J Nucl Med* 1988; 29:324–328
55. Schirrmeister H, Guhlmann A, Kotzerke J, et al. Early detection and accurate description of extent of metastatic bone disease in breast cancer with fluoride ion and positron emission tomography. *J Clin Oncol* 1999; 17:2381–2389
56. Kwee TC, Kwee RM, Nievelstein RA. Imaging in staging of malignant lymphoma: a systematic review. *Blood* 2008; 111:504–516
57. Wu HC, Yen RF, Shen YY, Kao CH, Lin CC, Lee CC. Comparing whole body ^{18}F-2-deoxyglucose positron emission tomography and technetium-99m methylene diphosphate bone scan to detect bone metastases in patients with renal cell carcinomas: a preliminary report. *J Cancer Res Clin Oncol* 2002; 128:503–506
58. Hsia TC, Shen YY, Yen RF, Kao CH, Changlai SP. Comparing whole body ^{18}F-2-deoxyglucose positron emission tomography and technetium-99m methylene diophosphate bone scan to detect bone metastases in patients with non-small cell lung cancer. *Neoplasma* 2002; 49:267–271
59. Wafaie AKH, Kotb M, Zeitoun R, Ismail S. Evaluation of the efficiency of FDG PET/CT in detection and characterization of skeletal metastases. *Egyptian J Radiol Nucl Med* 2014; 45:181–190
60. Bredella MA, Steinbach L, Caputo G, Segall G, Hawkins R. Value of FDG PET in the assessment of patients with multiple myeloma. *AJR* 2005; 184:1199–1204
61. Shortt CP, Gleeson TG, Breen KA, et al. Whole-body MRI versus PET in assessment of multiple myeloma disease activity. *AJR* 2009; 192:980–986
62. Ito S, Kato K, Ikeda M, et al. Comparison of 18F-FDG PET and bone scintigraphy in detection of bone metastases of thyroid cancer. *J Nucl Med* 2007; 48:889–895
63. Long NM, Smith CS. Causes and imaging features of false positives and false negatives on F-PET/CT in oncologic imaging. *Insights Imaging* 2011; 2:679–698
64. Wong KK, Piert M. Dynamic bone imaging with ^{99m}Tc-labeled diphosphonates and ^{18}F-NaF: mechanisms and applications. *J Nucl Med* 2013; 54:590–599
65. Ak I, Onner H, Akay OM. Is there any complimentary role of F-18 NaF PET/CT in detecting of osseous involvement of multiple myeloma? A comparative study for F-18 FDG PET/CT and F-18 FDG NaF PET/CT. *Ann Hematol* 2015; 94:1567–1575
66. Schirrmeister H, Guhlmann A, Elsner K, et al. Sensitivity in detecting osseous lesions depends on anatomic localization: planar bone scintigraphy versus ^{18}F PET. *J Nucl Med* 1999; 40:1623–1629
67. Waitches G, Zawin JK, Poznanski AK. Sequence and rate of bone marrow conversion in the femora of children as seen on MR imaging: are accepted standards accurate? *AJR* 1994; 162:1399–1406
68. Vogler JB 3rd, Murphy WA. Bone marrow imaging. *Radiology* 1988; 168:679–693
69. Dawson KL, Moore SG, Rowland JM. Age-related marrow changes in the pelvis: MR and anatomic findings. *Radiology* 1992; 183:47–51
70. Dooms GC, Fisher MR, Hricak H, Richardson M, Crooks LE, Genant HK. Bone marrow imaging: magnetic resonance studies related to age and sex. *Radiology* 1985; 155:429–432
71. Poulton TB, Murphy WD, Duerk JL, Chapek CC, Feiglin DH. Bone marrow reconversion in adults who are smokers: MR imaging findings. *AJR* 1993; 161:1217–1221
72. Swartz PG, Roberts CC. Radiological reasoning: bone marrow changes on MRI. *AJR* 2009; 193(suppl 3):S1–S4; quiz, S5–S9
73. Seiderer M, Staebler A, Wagner H. MRI of bone marrow: opposed-phase gradient-echo sequences with long repetition time. *Eur Radiol* 1999; 9:652–661
74. Shah GL, Rosenberg AS, Jarboe J, Klein A, Cossor F. Incidence and evaluation of incidental abnormal bone marrow signal on magnetic resonance imaging. *ScientificWorldJournal* 2014; 2014:380814
75. Taira AV, Herfkens RJ, Gambhir SS, Quon A. Detection of bone metastases: assessment of integrated FDG PET/CT imaging. *Radiology* 2007; 243:204–211
76. Damron TA, Morgan H, Prakash D, Grant W, Aronowitz J, Heiner J. Critical evaluation of Mirels' rating system for impending pathologic fractures. *Clin Orthop Relat Res* 2003; S201–S207
77. Mirels H. Metastatic disease in long bones: a proposed scoring system for diagnosing impending pathologic fractures. *Clin Orthop Relat Res* 1989; 256–264
78. Liu PT, Valadez SD, Chivers FS, Roberts CC, Beauchamp CP. Anatomically based guidelines for core needle biopsy of bone tumors: implications for limb-sparing surgery. *RadioGraphics* 2007; 27:189–205; discussion, 206

(Figures start on next page)

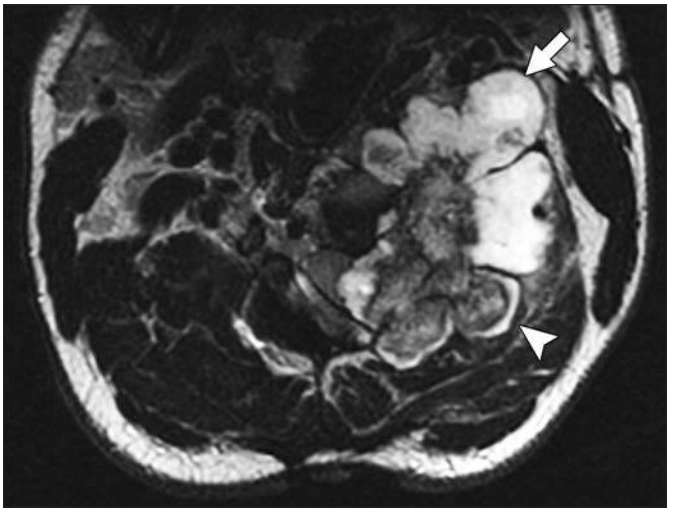

Fig. 1—32-year-old man with cervical osteochondroma showing growth and increased pain over prior 6 months. Axial T2-weighted (TR/TE, 6566/117) MR image shows osteochondroma along left lateral cervical spine. Note thin cartilage cap posteriorly (*arrowhead*) and thickened cartilage cap anteriorly (> 2 cm) representing secondary chondrosarcoma (*arrow*).

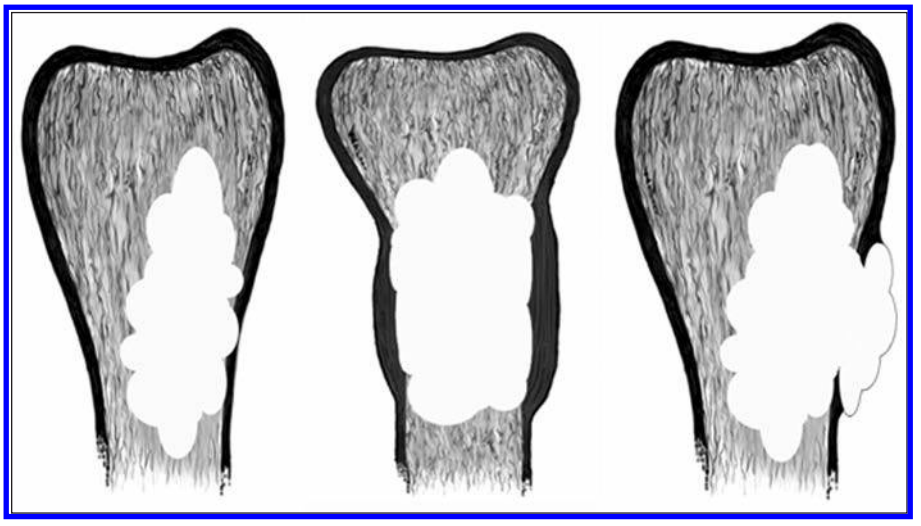

Fig. 2—Illustrations of aggressive features in chondroid lesions. Left illustration shows deep (greater than two-thirds) endosteal scalloping of cortex. Middle illustration shows expansile cortical remodeling. Right illustration shows cortical destruction and soft-tissue extension of lesion. (Drawings by Walker E)

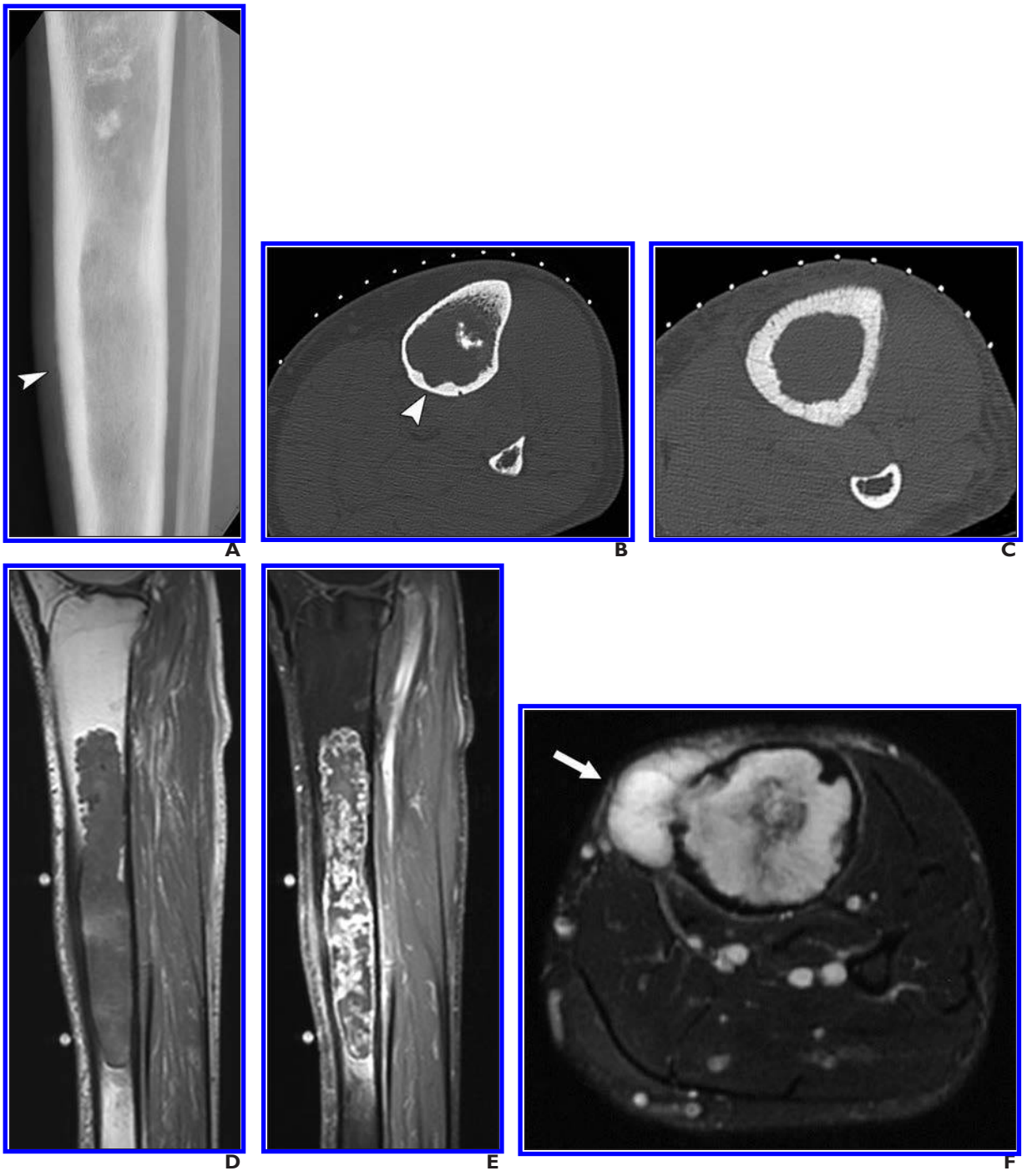

Fig. 3—52-year-old woman with central medullary grade 2 chondrosarcoma.
A, Lateral radiograph of tibia reveals chondroid matrix of superior aspect of lesion (*arrowhead*). Inferior component is causing expansile remodeling of tibial cortex and subtle periosteal reaction.
B and **C,** Axial CT images obtained proximally (**B**) and distally (**C**) during biopsy show deep (greater than two-thirds) endosteal scalloping (*arrowhead*, **B**) of cortex and show cortical tunneling and periosteal reaction (**C**).
D, Sagittal T1-weighted MRI sequence shows lobular growth at superior aspect of lesion, likely representing preexisting enchondroma. Inferior component is behaving more aggressively, causing expansile remodeling of tibial cortex.
E, IV gadolinium-enhanced T1-weighted fat-saturated MR image shows typical peripheral and septal enhancement pattern of chondroid lesions.
F, Axial T2-weighted fat-saturated MRI sequence shows cortical destruction and soft-tissue mass (*arrow*).

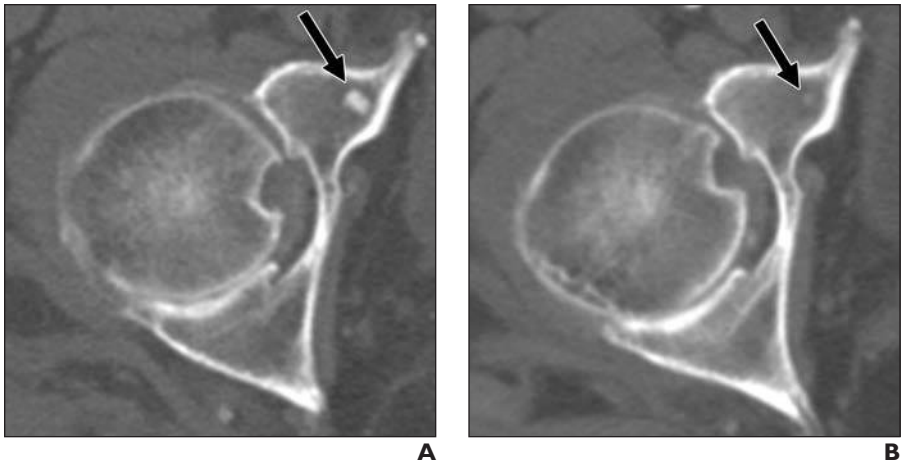

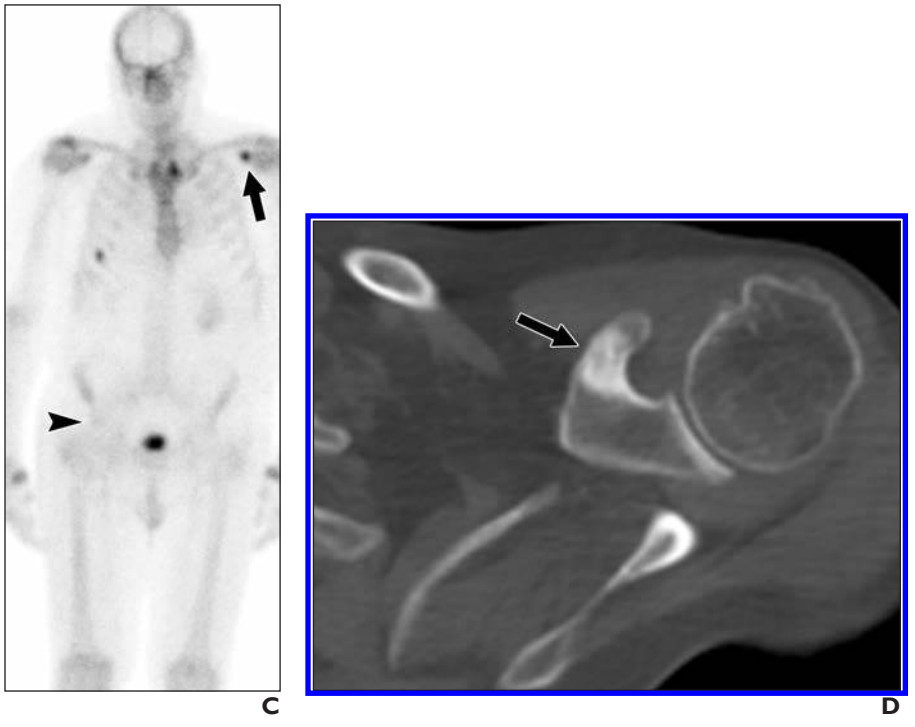

Fig. 4—83-year-old man with weight loss and fatigue.
A and **B,** Axial CT images of right hip obtained 1.5 years apart show sclerotic focus (*arrows*). Follow-up image (**A**) shows that focus has enlarged over 400% compared to initial image obtained 1.5 years earlier (**B**).
C, Although acetabular lesion is not able to be detected on planar bone imaging (*arrowhead*), separate suspicious focus (*arrow*) was identified in left scapula.
D, CT of left shoulder shows mildly inhomogenous sclerotic lesion in coracoid (*arrow*) serving as more accessible biopsy site for establishing this patient's diagnosis of metastatic prostate cancer.

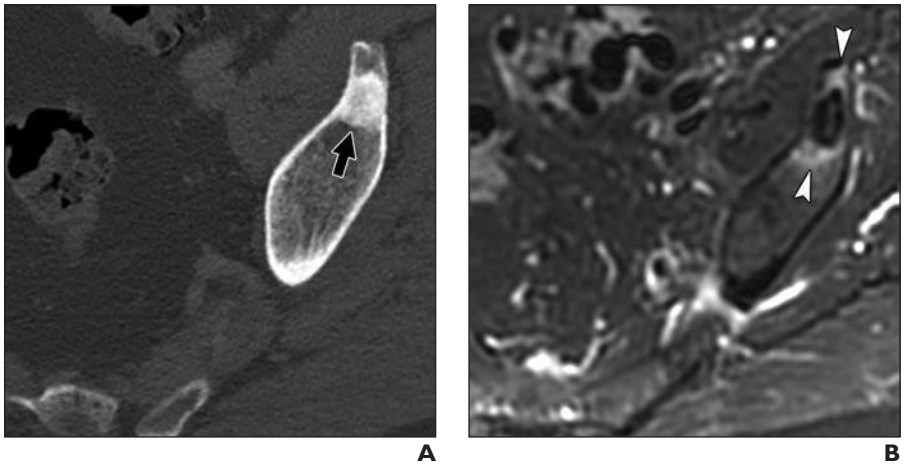

Fig. 5—57-year-old man with incidentally identified sclerotic lesion.
A and **B,** Lesion is seen on axial CT (*arrow*, **A**) and axial T2-weighted fat-suppressed MR image (**B**). Abnormal halo of increased T2 signal (*arrowheads*, **B**) surrounds lesion, which was shown to be prostate cancer on biopsy.

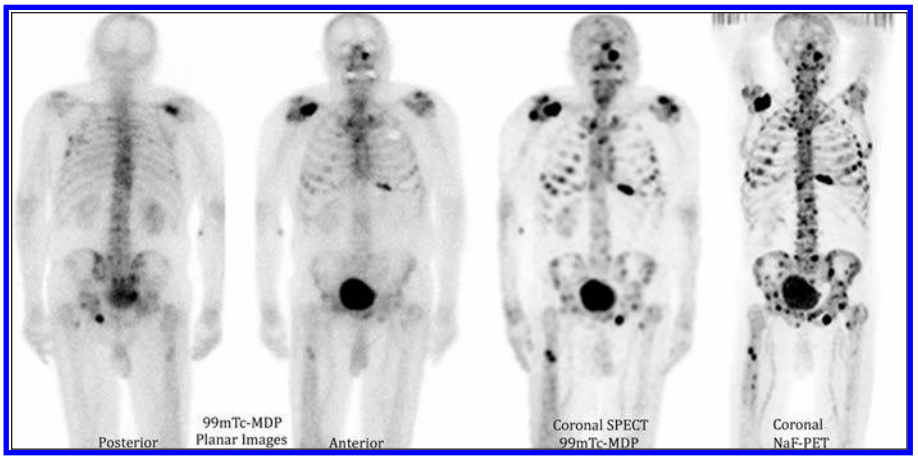

Fig. 6—72-year-old man with metastatic prostate cancer. From left to right, images show comparison of detection of metastatic bone lesions on planar bone scintigraphy (posterior and anterior views), SPECT scintigraphy, and ^{18}F-NaF-PET. Conspicuity and number of lesions visible increases from planar imaging to SPECT to ^{18}F-NaF-PET. MDP = methylene diphosphonate. (Courtesy of Osborne JR, Memorial Sloan Kettering Cancer Center, New York, NY)

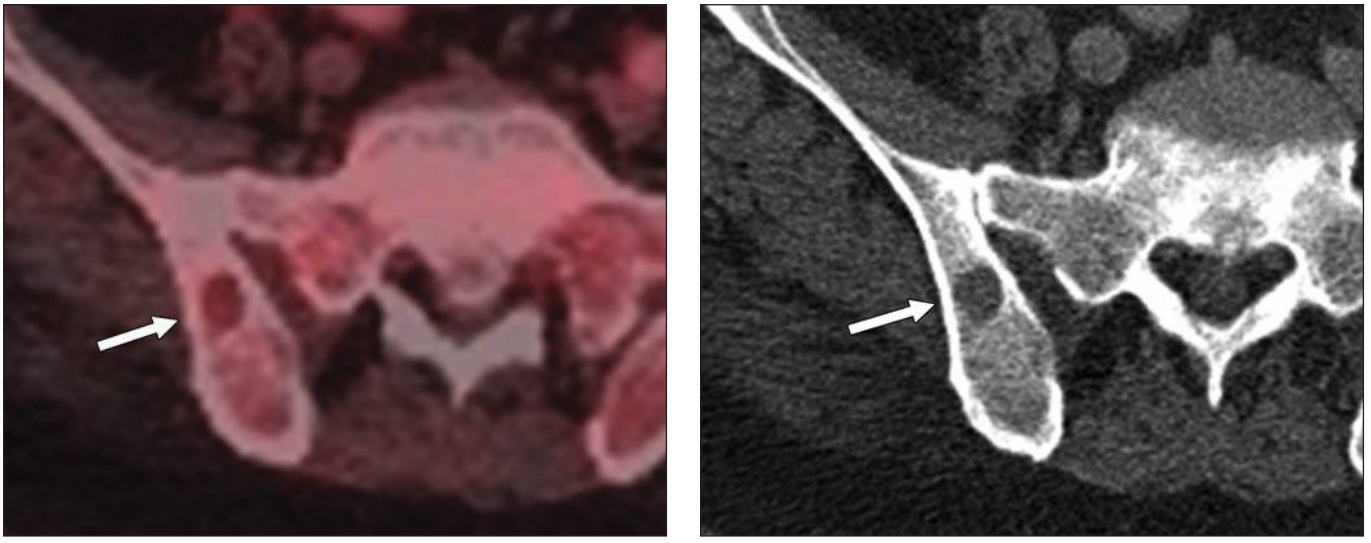

Fig. 7—70-year-old man with newly diagnosed colon cancer. Osteolytic lesion lacking sclerotic margin was found in posterior right iliac wing.
A, Lesion (*arrow*) lacked metabolic activity on initial staging FDG PET/CT and so was followed instead of biopsied.
B, On unenhanced axial CT image, lesion (*arrow*) remained stable in size at 2 years with no systemic therapy and was presumed to represent benign fibroosseous lesion.

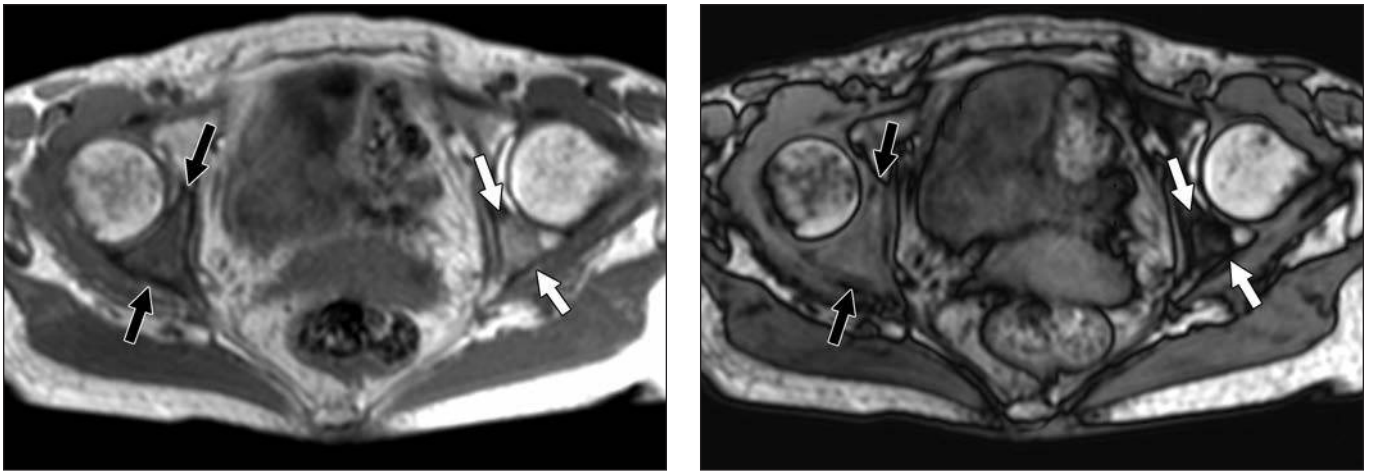

Fig. 8—63-year-old woman with metastatic gastric carcinoma.
A and **B,** Gradient T1-weighted in-phase (**A**) and out-of-phase (**B**) axial MR images were obtained through pelvis. Focal area of rounded red marrow in posterior left acetabulum (*white arrows*) is seen to lose more signal than muscle on out-of-phase images because of intravoxel marrow fat. Gastric metastasis in right posterior acetabulum (*black arrows*) shows India ink artifact anteriorly at interface with normal marrow but does not decrease in signal because of tumor displacing normal marrow fat.

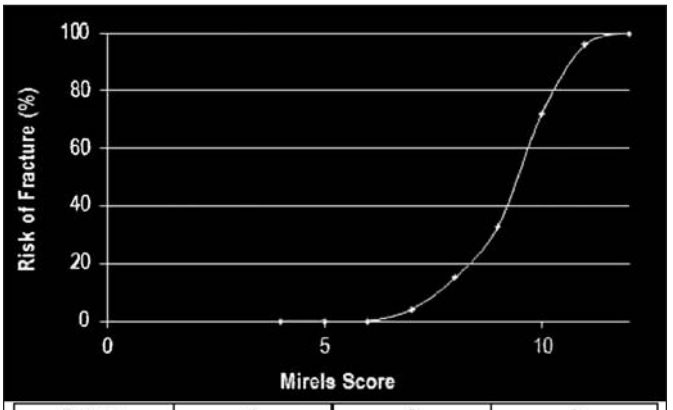

Points	1	2	3
Location	Upper Extremity	Lower Extremity	Peritrochanteric
Appearance	Osteoblastic	Mixed	Osteolytic
Cortical Involvement	<1/3rd	1/3rd – 2/3rd	>2/3rds
Pain	Mild	Moderate	Functional

Fig. 9—Mirels scoring of fracture risk. Graph of fracture risk was reconstructed from original published data [77].

FOR YOUR INFORMATION

This article is available for CME and Self-Assessment (SA-CME) credit that satisfies Part II requirements for maintenance of certification (MOC). To access the examination for this article, follow the prompts associated with the online version of the article.

This article has been cited by:

1. Julia Crim. 2023. Bone radiographs: sometimes overlooked, often difficult to read, and still important. *Skeletal Radiology* **46**. . [Crossref]
2. Ryan Thompson, Noushin Vahdat, Wael Alshehri, Lejla Aganovic, Saif Baig, Sara Mirza, Holly Cassidy, Fiona Hughes. 2023. Beyond the abdominal and pelvic cavity: abdominal wall and spinal "Aunt Minnies". *Abdominal Radiology* **48**:4, 1479-1504. [Crossref]
3. Julia Crim, Lester J. Layfield. 2023. Bone and soft tissue tumors at the borderlands of malignancy. *Skeletal Radiology* **52**:3, 379-392. [Crossref]
4. Aaron Jen, Jeanne Kochkodan-Self, Jacob C Mandell. 2023. A Retrospective Analysis of Sternal Lesions Detected on Breast MRI in Patients Without History of Cancer. *Journal of Breast Imaging* **5**:1, 48-55. [Crossref]
5. Sigfred Lajara. Bone 301-328. [Crossref]
6. Michael A. Via, Ilya Iofin, Jerry Liu, Jeffrey I. Mechanick. Skeletal Complications 1-14. [Crossref]
7. Connie Y. Chang, Hillary W. Garner, Shivani Ahlawat, Behrang Amini, Matthew D. Bucknor, Jonathan A. Flug, Iman Khodarahmi, Michael E. Mulligan, Jeffrey J. Peterson, Geoffrey M. Riley, Mohammad Samim, Santiago A. Lozano-Calderon, Jim S. Wu. 2022. Society of Skeletal Radiology– white paper. Guidelines for the diagnostic management of incidental solitary bone lesions on CT and MRI in adults: bone reporting and data system (Bone-RADS). *Skeletal Radiology* **51**:9, 1743-1764. [Crossref]
8. Erique Pinto1, Diana Penha1,2, Bruno Hochhegger3, Colin Monaghan2, Edson Marchiori4,5, Luís Taborda-Barata1, Klaus Irion2. 2022. Incidental chest findings on coronary CT angiography: a pictorial essay and management proposal. *Jornal Brasileiro de Pneumologia* e20220015. [Crossref]
9. Ryan J. Hoffman, Rupert O. Stanborough, Hillary W. Garner. 2022. Diagnostic Imaging Approach to Solitary Bone Lesions. *Seminars in Roentgenology* **57**:3, 241-251. [Crossref]
10. Lina GARCÍA CAÑAMAQUE, Caroline A. FIELD, Felipe S. FURTADO, Isabel PLAZA DE LAS HERAS, Jad S. HUSSEINI, Rene BALZA, Mohamed JARRAYA, Onofrio A. CATALANO, Merche MITJAVILA CASANOVAS. 2022. Contribution of positron emission tomography/magnetic resonance imaging in musculoskeletal malignancies. *The Quarterly Journal of Nuclear Medicine and Molecular Imaging* **66**:1. . [Crossref]
11. Joao R. T. Vicentini, Sina Habibollahi, Ambrose J. Huang, Connie Y. Chang. Image-Guided Biopsy and Intervention for Metastatic Disease 323-333. [Crossref]
12. Marko Bergovec, Jörg Friesenbichler, Maria Smolle, Andreas Leithner. Grundlegende Aspekte pädiatrischer Tumoren 1-13. [Crossref]
13. Carlos R. Goulart, Aladine A. Elsamadicy, Tobias A. Mattei, Benjamin C. Reeves, Michael A. Weicker, Michele H. Johnson, Ehud Mendel. Neuroimaging for surgical treatment planning of neoplastic disease of the spine 871-891. [Crossref]
14. Hoiwan Cheung, Alekhya Yechoor, Fatemeh Behnia, Alireza Behrad Abadi, Iman Khodarahmi, Maryam Soltanolkotabi, Mehrzad Shafiei, Majid Chalian. 2022. Common Skeletal Neoplasms and Nonneoplastic Lesions at 18 F-FDG PET/CT. *RadioGraphics* **42**:1, 250-267. [Crossref]
15. Jeanette Ansholm Hansen, Mohammad Naghavi-Behzad, Oke Gerke, Christina Baun, Kirsten Falch, Sandra Duvnjak, Abass Alavi, Poul Flemming Høilund-Carlsen, Malene Grubbe Hildebrandt. 2021. Diagnosis of bone metastases in breast cancer: Lesion-based sensitivity of dual-time-point FDG-PET/CT compared to low-dose CT and bone scintigraphy. *PLOS ONE* **16**:11, e0260066. [Crossref]
16. Keaton Rummel, John Benson, Luke Roller. 2021. Prostate adenocarcinoma with osteolytic metastases: Case report and review of the literature. *Radiology Case Reports* **16**:11, 3565-3568. [Crossref]
17. Nicholas G. Zaorsky, Jeremie Calais, Stefano Fanti, Derya Tilki, Tanya Dorff, Daniel E. Spratt, Amar U. Kishan. 2021. Salvage therapy for prostate cancer after radical prostatectomy. *Nature Reviews Urology* **18**:11, 643-668. [Crossref]
18. Jignesh Shah, Ankita Chauhan. Imaging of Pediatric Benign Bone Tumors . [Crossref]
19. Mine B Lange, Lars J Petersen, Michael B Nielsen, Helle D Zacho. 2021. Validity of negative bone biopsy in suspicious bone lesions. *Acta Radiologica Open* **10**:7, 205846012110306. [Crossref]
20. Jignesh Shah, Darshan Gandhi, Ankita Chauhan, Saurabh Gupta. 2021. Imaging Review of Pediatric Benign Osteocytic Tumors and Latest Updates on Management. *Journal of Clinical Medicine* **10**:13, 2823. [Crossref]

21. Jeffrey Levine, Iva Petkovska, Jonathan Landa, David D. B. Bates, Marinela Capanu, J. Louis Fuqua, Viktoriya Paroder, Junting Zheng, Marc J. Gollub, Jennifer S. Golia Pernicka. 2021. Bone lesions on baseline staging rectal MRI: prevalence and significance in patients with rectal adenocarcinoma. *Abdominal Radiology* **46**:6, 2423-2431. [Crossref]
22. Vaibhav Gulati, Majid Chalian, Jaehyuck Yi, Uma Thakur, Avneesh Chhabra. 2021. Sclerotic bone lesions caused by non-infectious and non-neoplastic diseases: a review of the imaging and clinicopathologic findings. *Skeletal Radiology* **50**:5, 847-869. [Crossref]
23. Jad S. Husseini, Bárbara Juarez Amorim, Angel Torrado-Carvajal, Vinay Prabhu, David Groshar, Lale Umutlu, Ken Herrmann, Lina García Cañamaque, José Ramón García Garzón, William E. Palmer, Pedram Heidari, Tiffany Ting-Fang Shih, Jacob Sosna, Cristina Matushita, Juliano Cerci, Marcelo Queiroz, Valdair Francisco Muglia, Marcello H. Nogueira-Barbosa, Ronald J. H. Borra, Thomas C. Kwee, Andor W. J. M. Glaudemans, Laura Evangelista, Marco Salvatore, Alberto Cuocolo, Andrea Soricelli, Christian Herold, Andrea Laghi, Marius Mayerhoefer, Umar Mahmood, Ciprian Catana, Heike E. Daldrup-Link, Bruce Rosen, Onofrio A. Catalano. 2021. An international expert opinion statement on the utility of PET/MR for imaging of skeletal metastases. *European Journal of Nuclear Medicine and Molecular Imaging* **48**:5, 1522-1537. [Crossref]
24. Allison Herring, Derik L. Davis. 2021. Mimickers of Hill-Sachs Lesions. *Canadian Association of Radiologists Journal* **72**:2, 258-270. [Crossref]
25. Jorge Vaz Lourenço, Joana Coelho, Andrea Salgueiro. 2021. Enostosis-related epilepsy. *BJR|case reports* **7**:3, 20200152. [Crossref]
26. Antoine Azar, Hillary W. Garner, Nicholas G. Rhodes, Bhavya Yarlagadda, Daniel E. Wessell. 2021. CT Attenuation Values Do Not Reliably Distinguish Benign Sclerotic Lesions From Osteoblastic Metastases in Patients Undergoing Bone Biopsy. *American Journal of Roentgenology* **216**:4, 1022-1030. [Abstract] [Full Text] [PDF] [PDF Plus]
27. Charles H. Bush. 2021. Editorial Comment on "CT Attenuation Values Do Not Reliably Distinguish Benign Sclerotic Lesions From Osteoblastic Metastases in Patients Undergoing Bone Biopsy". *American Journal of Roentgenology* **216**:4, 1030-1030. [Citation] [Full Text] [PDF] [PDF Plus]
28. M.R. Nouh, Ahmed Doweidar, Abdullah Mohie-Eddin Khalil. 2021. Apparent diffusion coefficient (ADC): A potential in vivo biological surrogate of the incidentally discovered bone lesions at 3T MRI. *European Journal of Radiology Open* **8**, 100386. [Crossref]
29. Phichayut Phinyo, Titinat Maihom, Areerak Phanphaisarn, Pakorn Kerdsinchai, Ekarat Rattarittamrong, Jayanton Patumanond, Dumnoensun Pruksakorn. 2020. Development of a clinical diagnostic tool to differentiate multiple myeloma from bone metastasis in patients with destructive bone lesions (MM-BM DDx). *BMC Family Practice* **21**:1. . [Crossref]
30. Ryan D. Meek, Megan K. Mills, Christopher J. Hanrahan, Brooke R. Beckett, Richard L. Leake, Hailey Allen, Don D. Williams, Matthew Tommack, Sandra Schmahmann, Barry G. Hansford. 2020. Pearls and Pitfalls for Soft-Tissue and Bone Biopsies: A Cross-Institutional Review. *RadioGraphics* **40**:1, 266-290. [Crossref]
31. Richard A. Marshall, Jacob C. Mandell, Michael J. Weaver, Marco Ferrone, Aaron Sodickson, Bharti Khurana. 2018. Imaging Features and Management of Stress, Atypical, and Pathologic Fractures. *RadioGraphics* **38**:7, 2173-2192. [Crossref]